Time-resolved ellipsometry for studies of heat transfer at liquid/solid and gas/solid interfaces

Chang-Ki Min, David G. Cahill, and Steve Granick
Department of Materials Science and Engineering, and Frederick Seitz Materials Research Laboratory, University of Illinois, Urbana, Illinois 61801, USA

(Received 23 November 2009; accepted 28 June 2010; published online 28 July 2010)

We describe a sensitive method for measuring time-dependent changes in refractive index within ~5 μm of an interface using off-null time-resolved ellipsometry and a dual-cavity femtosecond laser. The sensitivity to changes in refractive index is two orders of magnitude higher than conventional picosecond interferometry. A thin metal film on a sapphire substrate is heated by ~10 K using an ultrafast optical pump pulse; the subsequent changes of the phase difference $\delta\Delta$ between $\hat{p}$ and $\hat{s}$ polarized reflectivity are tracked using off-null ellipsometry using a time-delayed probe pulse. We demonstrate a sensitivity of $\delta\Delta \approx 3\times10^{-7}$ deg/$\sqrt{\text{Hz}}$ using interfaces between Au and water, and Au and various gases including R134a, a common refrigerant. Our data for the damping rate of ≈200 MHz frequency acoustic waves in O_2, N_2, and Ar at atmospheric pressure agree well with prior results obtained at much lower pressures and frequencies. © *2010 American Institute of Physics.* [doi:10.1063/1.3465329]

I. INTRODUCTION

The science of interfaces—and the tools needed to characterize interfaces—are not as fully developed as their counterparts for the bulk. Here, motivated by the fact that measurements of the transport of heat at interfaces can provide a powerful tool for studying physical state of interfaces,[1] we describe a sensitive method to probe thermally induced changes in refractive index in the region that lies within a few microns of a liquid/solid or gas/solid interface. Our method is based on off-null ellipsometry and provides a time-resolution of ~100 fs using a dual-cavity Ti:sapphire laser.

Time-resolved ellipsometry has been applied previously in studies of fast electronic and structural relaxation of semiconductors and metals; typically, time-resolved ellipsometry provides higher sensitivity to optical constants than time-resolved reflectometry.[2–9] With the use of femtosecond laser sources, subpicosecond time resolution is easily achieved but the signal-to-noise is often a limiting factor in the measurement. Several studies describe methods to improve the sensitivity of time-resolved ellipsometry by optimizing the optical configuration.[5–7] A common implementation involves the use of a polarizing beamsplitter configured to maximize the change in the optical power[7–9] $dP/d\eta$, where P is the optical power on photodetector and η is the ellipticity.

We describe further improvements in the sensitivity that enables high-precision measurements of changes of the refractive index of liquids and even gases adjacent to a abruptly heated surface. We show that the off-null geometry provides an order of magnitude improvement in sensitivity compared to other approaches.[7] Furthermore, rapid scanning of the pump-probe delay time using a dual-cavity laser system improves the sensitivity by another order of magnitude. Customarily, the disadvantage of the off-null geometry is heating created by high laser fluence incident on the sample. Alleviating this, we coat the Ti heating layer with a highly reflective Au coating to minimize heating by the probe and reduce background signals from the solid surface.

Consider a gas or liquid in contact with a planar thin metal film that is abruptly heated by an optical pulse. Two classes of phenomena must be taken into account: heat transfer and the propagation of acoustic waves. The thermal and acoustic phenomena are, of course, coupled: the amplitude and phase of the acoustic wave generated at an interface are at least partly controlled by the rate of heat transfer across the interface. Heat moving from the metal film into the fluid increases the temperature of the fluid; the resulting thermal expansion of the fluid contributes to the amplitude and phase of the acoustic wave.[10]

Time-resolved ellipsometry offers advantages in ultrafast heat transfer experiments in comparison with time-domain thermoreflectance[1,11] (TDTR) or picosecond interferometry, approaches used by our laboratory and others.[12,13] In a typical TDTR experiment, a metal layer is heated by a pump optical pulse and the thermal relaxation of the metal layer is monitored through transient changes in optical reflectivity. The optical reflectivity of most metals depends on temperature. Changes in optical reflectivity are therefore linearly related to temperature if the temperature excursion is small. TDTR measures the decay of the temperature of the same layer that is heated; i.e., the heat source and thermometer are the same component of the system. In time-resolved ellipsometry, the heat source is, as in TDTR, optical absorption by a thin metal film, but the transfer of heat is probed through changes in the index of refraction of the adjacent material. Separating the heat source and temperature measurement provides enhanced sensitivity because the signal starts from zero and grows rather than starting at a high value and decaying.

Picosecond interferometry—also known as time-domain

 © 2010 American Institute of Physics

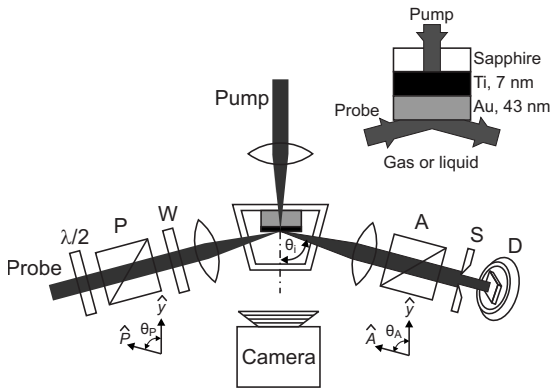

FIG. 1. Schematic drawing of the time-resolved ellipsometer. P: polarizer; W: λ/4 wave-plate; A: analyzer; S: slit; D: silicon photodiode. The inset shows a magnified view of the sample.

Brillouin scattering—has been used extensively in studies of acoustic waves generated at an interface; the majority of this prior work has focused on the use of these acoustic waves in studies of the elasticity of materials and the thickness of thin films.[14,15] Picosecond interferometry has also been used to study gigahertz acoustics of liquids. Measurements of the reflectance of solid-glycerol interfaces at 100–300 GHz were compared to the predictions of the acoustic mismatch model.[16] The dispersion and attenuation of 20–90 GHz shear and longitudinal acoustic waves were related to relaxation dynamics in this frequency range.[17]

In the following, we analyze the signal acquired in time-resolved ellipsometry using a Jones matrix formalism[18,19] and demonstrate our approach on a model system, the Au/water interface, in which acoustic waves are predominately created by thermal expansion of the solid substrate and wave propagation into the adjacent water. Because of the small thermal expansion coefficient and small thermal diffusivity of water, heat transfer does not contribute significantly to the generation of the acoustic wave. We then show that off-null ellipsometry provides orders of magnitude more sensitivity than a detection scheme that utilizes a $\hat{p}$ or $\hat{s}$ linearly polarized probe. Finally, the utility of our time-resolved ellipsometer is further demonstrated using data for several gases. The thermal expansion coefficient of gases is large and the transmittance of acoustic wave from solid to gas is small; therefore, acoustic waves in the gas are predominately created by heat transfer at the solid-gas interface.[20]

II. TIME-RESOLVED ELLIPSOMETRY USING OFF-NULL GEOMETRY

The off-null ellipsometry geometry reduces background and improves the signal-to-noise ratio when compared to the use of a polarizing beamsplitter to determine the polarization state of the probe.[7–9] A schematic diagram of the sample structure and the optical layout is shown in Fig. 1. Heat pulses are produced by the absorption of the pump beam in a thin film of Ti deposited on sapphire. To minimize the thermoreflectance signal generated by the heat source, a thin film of Au is deposited on top of Ti layer. The thicknesses of the Au and Ti layers are measured by Rutherford backscattering spectrometry.

Probe pulses are used to measure the resulting time-dependent change of the phase (Δ) between $\hat{p}$ and $\hat{s}$ polarized light at variable time delays relative to the pump pulses. Pump and probe pulses are generated by separate Ti:sapphire laser oscillators that coexist in a custom-built two-cavity laser setup; variable time delays between pump and probe pulses are generated by the small differences of the repetition rates of the two oscillators. (The repetition rates of the two mode-locked lasers are both ≈80 MHz.) The $1/e^2$ intensity radius of the focused pump and probe beams is $w_0 \approx 10\ \mu$m. For the pump laser powers that we typically employ 50–70 mW, the temperature rise created by one pump pulse is ≈10 K and the steady-state temperature rise created by the average laser power is ≈30 K.

A. Optical analysis

Ellipsometry measures the ratio of the Fresnel reflection coefficients of $\hat{p}$ and $\hat{s}$ polarized light (r_p/r_s). This ratio is, in general, a complex number; the amplitude and the phase of the ratio are usually decomposed as $r_p/r_s = \exp i\Delta \tan \Psi$.[18,19] Our implementation of time-resolved ellipsometry is related to certain types of imaging ellipsometers where the spatial variations of the thickness of a layer are obtained through changes in the intensity of light produced when the sample is translated in the x-y plane.[19] In imaging ellipsometry, the output data are the spatial variation in thickness; in time-resolved ellipsometry, the output data are the time evolution of changes in the ellipsometric parameters $\delta\Delta$ and $\delta\Psi$, induced by the pump optical pulses. These changes can be a small as $\delta\Delta < 10^{-2}$ which is equivalent to the change in phase created by a 3 pm thick layer of SiO_2 on Si at an angle of incidence of $\theta_i = 70°$ and optical wavelength of $\lambda = 632.8$ nm.

For the probe, we use a polarizer-compensator-sample-analyzer arrangement with a fixed compensator angle as shown in Fig. 1. The combination of a λ/2 wave-plate and polarizer selects the initial polarization and intensity of the incident light. The null position, where the signal in the photodiode is minimized, is obtained by adjusting the angle of the polarizer and analyzer. The slit reduces the spread of the incidence angle from 15° to 2°–5°.

Null ellipsometry is conveniently described using the Jones matrix formalism (see Refs. 18 and 19); we briefly summarize the main results here for completeness. For unity probe power on the sample, the electric field of $\hat{p}$ and $\hat{s}$ polarized light on the photodetector is given by

$$\begin{pmatrix} E_p \\ E_s \end{pmatrix} = R(-\theta_A)\begin{bmatrix} 0 & 0 \\ 0 & 1 \end{bmatrix} R(\theta_A) S C \begin{pmatrix} -\sin\theta_P \\ \cos\theta_P \end{pmatrix},$$

$$R(\theta) = \begin{bmatrix} \cos\theta & \sin\theta \\ -\sin\theta & \cos\theta \end{bmatrix}, \tag{1}$$

$$C = R\left(-\frac{\pi}{4}\right)\begin{bmatrix} e^{i\pi/4} & 0 \\ 0 & e^{-i\pi/4} \end{bmatrix} R\left(\frac{\pi}{4}\right),$$

where $R(\theta)$, S, and C are the frame rotation, sample, and quarter wave-plate matrices, and θ_A and θ_P are the counter-clockwise rotation angles of the analyzer and the polarizer

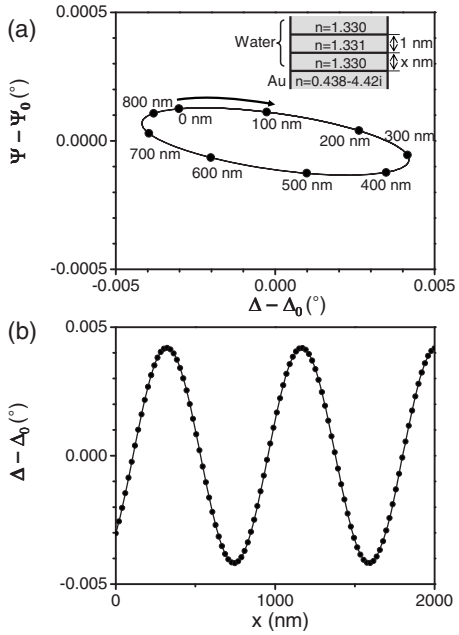

FIG. 2. Optical model for the effect of the propagation of an acoustic pulse on the ellipsometry parameters Ψ and Δ. The geometry of the model is shown as the inset to panel (a). Data in panel (a) are the simulation result as a function of the propagation distance of the acoustic pulse, x; Ψ_0 and Δ_0 are the ellipsometry parameters in the absence of the acoustic pulse. Panel (b) shows a comparison between the changes in Δ calculated directly from the model (solid line) and the changes in Δ derived indirectly (filled symbols) by the simulation of our measurement.

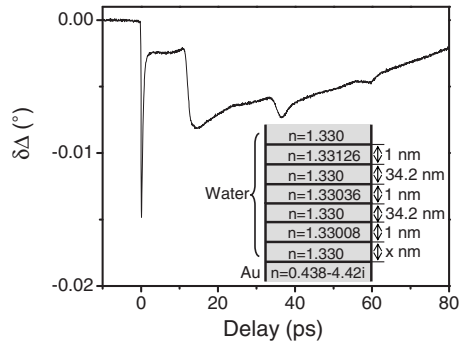

FIG. 3. The acoustic signal from the Au film measured at short time is used as an input to simulate the acoustic wave that enters water. The inset shows the geometry of a simulation model: three acoustic pulses are modeled as three layers in water with corresponding distances and proportional values of the index of refraction.

from the out-of-plane axis (see Fig. 1). The fast axis of the quarter wave-plate is rotated by $\pi/4$ from the horizontal plane. The rotation direction of the quarter wave-plate is chosen arbitrarily and its counter-rotation affects only the shift of null positions.

The sample matrix is diagonal and can be represented by the Fresnel coefficients or, equivalently, by the ellipsometry parameters,

$$S = \begin{bmatrix} r_p & 0 \\ 0 & r_s \end{bmatrix} = \frac{r_s}{\cos \Psi} \begin{bmatrix} \sin \Psi e^{i\Delta} & 0 \\ 0 & \cos \Psi \end{bmatrix}. \quad (2)$$

The Fresnel reflection coefficients, r_p and r_s, that appear in Eq. (2) are generally derived as a function of λ and θ_i using a multilayer optical model. We use the program source code from Ref. 19. The null positions of the angle of polarizer and analyzer in the region, $0 < \theta_A < \pi/2$, are easily related to the ellipsometry parameters: $\Delta = 3\pi/2 - 2\theta_P$ and $\Psi = \pi/2 - \theta_A$. Using Eqs. (1) and (2), we calculate the signal intensity at the photodiode as $P = |E_p|^2 + |E_s|^2$.

We begin our analysis of the experiments by considering how the propagation of an acoustic pulse transmitting from Au into water modifies the off-null signal. The acoustic pulse in water corresponds to a thin layer of water at higher pressure than ambient. This change in pressure creates a change in density and index of refraction. As a function of time, the thin layer of water with higher index moves farther away from the interface at the longitudinal speed of sound, $\nu_l = 1497$ m/s at 25 °C.[21]

We calculate how the motion of this thin layer alters the Fresnel coefficients using a thin layer optical model that is illustrated by the inset to Fig. 2(a): $n_{\mathrm{Au}} = 0.438 - 4.42i$, $n_{\mathrm{water}} = 1.33$, $\lambda = 740$ nm, $\theta_i = 70.8°$, and 1 nm thick layer of $n_{\mathrm{layer}} = 1.331$ moving at the speed of sound. $\Psi_0 = 42.5°$ and $\Delta = 104.0°$ are calculated in the absence of an acoustic pulse and n_{Au} is measured using a commercial ellipsometer. The scale of the x-axis in Fig. 2(a) is ten times larger than the scale of the y-axis. The main effect of the acoustic pulse is to produce a change in Δ that oscillates around the null as the acoustic pulse propagates. Changes in Δ are >30 times larger than changes in Ψ. This result is expected because, in general, a higher density layer affects mainly the phase and not the amplitude.

The predominance of changes in Δ over changes in Ψ enables a unique conversion between the measured changes in intensity P and changes in Δ using a calculated conversion factor, $\beta = dP/d\Delta$. Although β increases linearly with the deviation of Δ from the null, β is approximately constant over the small range of Δ created by the acoustic pulse. In Fig. 2(b), we compare the model simulation results based on our measurement scheme at $\theta_P = \text{null} + 5°$ and values derived directly from Fresnel coefficients; the agreement is excellent.

In our experiments, the off-null signal is measured with nulling θ_A and off-nulling θ_P typically by 5°–8°, and calibrated using the quadratic fitting of measured P and off-null angle of θ_P without generating acoustic wave. The angles are θ_P and $\theta_A = 91.5°$ and 47.6° at the water interface, and 88.0° and 47.8° at the gas interface, respectively. Under these conditions, light is incident on the sample is approximately circularly polarized.

We compare experimental data and calculations for the Au/water interface in Figs. 3 and 4. The discussion of the ellipsometry signals above does not include contributions from changes in the index of refraction of Au or contributions from the changes in the temperature of water near the interface. Contributions to the signal from Au include a fast electronic response, a slow thermal response, and longitudinal acoustic waves that reflect between the surface and the Au/Ti/sapphire interface. Contributions from water include the slow temperature rise and temperature decay of water, and the longitudinal acoustic waves discussed above. The frequency of the oscillation in the signal, often referred to as the Brillouin frequency, is given by $f = \lambda/(2n_{\mathrm{water}} v_l \cos \theta_i)$. The initial phase of the signal oscillation is determined by

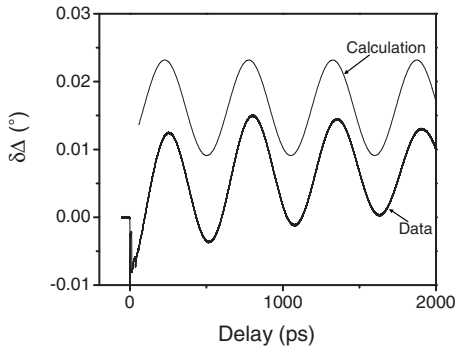

FIG. 4. Comparison of measured and simulated phase Δ of the acoustic wave in time-resolved ellipsometry for a Au film in contact with water. Changes in Δ are plotted against delay time between pump and probe optical pulses.

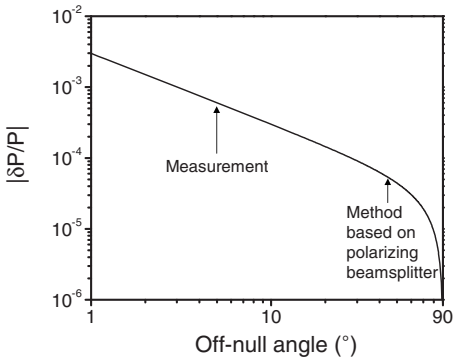

FIG. 5. Sensitivity of time-resolved ellipsometry calculated at time zero using the same conditions as described in Fig. 2. An inverse dependence of $\delta P/P$, which is probe power change δP induced by the pump pulses normalized by the total power P incident on the photodiode, is predicted with respect to off-null angle. The arrow indicates the off-null angle of ≈5° selected for typical experiments and 45° used for the method based on a polarizing beamsplitter.

the measurement geometry (θ_A and θ_P) and the mechanisms that generate the acoustic wave.

To calculate the contribution from the acoustic wave, we assume that the generation of the acoustic wave is caused only by expansion of the metal film and we neglect any contribution from the thermal expansion of water. Figure 3 shows the data for small values of the delay time between pump and probe where three peaks are visible at 12.1, 35.1, and 58.1 ps with amplitudes of 6.3×10^{-3}, 1.8×10^{-3}, and 4.2×10^{-4}, respectively. We interpret the first peak as the transit time of acoustic pulse generated in the Ti layer to the front surface of Au; the second and third peaks correspond to one and two round trip times between the front and back surface of the Au film.

The relative amplitude and delay time of three acoustic peaks are used to simulate the ellipsometry data at long times using the moving thin layer model as shown in the inset of Fig. 3. The delay time of acoustic peaks is converted to the position of thin layers using the speed of sound, $v_l = 1541$ m/s, measured in this experiment. The thickness of layers is chosen to be 1 nm which is $\approx\tau_{ac}v_l$, where τ_{ac} is the acoustic pulse width shown in Fig. 3. The proportional value for the modulation of refractive index is chosen to mimic the experimental data. The distance x is converted to pump-probe delay by the same speed of sound; the initial offset in the delay time is 58.4 ps given by the sum of time for the third acoustic peak and the acoustic travel time across 0.5 nm. This simulation, see Fig. 4, is in good agreement with the data but is shifted to smaller delay times by 26 ps.

B. Dual-cavity laser to generate the optical pump and probe

Our pump-probe measurement does not employ the conventional means of varying the delay time using a mechanical stage as an optical delay line. Instead, the pump and probe pulses are generated by two different custom-built Ti:sapphire lasers, which operate at 80 MHz with slightly different repetition rates, $\Delta f \approx 300$ Hz.[22] The beating between the lasers automatically generates a delay time of 0–12.5 ns that repeats at a frequency Δf. The advantage of using a dual-cavity laser, rather than an optical delay line, is the elimination of artifacts created by variations in beam-size and drift in the overlap between the pump and probe beams as a function of delay time. A second advantage is that fast scanning over delay time reduces the sensitivity of the experiment to slow fluctuations of the laser power and within the sample, which we find can be a problem in complex fluid media.

To preserve the short pulse duration of the lasers, pulse dispersion within the optics is compensated using a pair of prisms. The cross-correlation of pump and probe is 100 fs. The two lasers operate at slightly different wavelengths, the pump at 800 nm and probe at 740 nm, so that the scattered light from the pump is easily suppressed using an optical short-pass filter.

The pump and probe beams are focused to a diameter of 20 μm although the shape of probe beam is highly elongated because of the glancing angle of incidence. The volume probed is the region of overlap between the incident and reflected probe beam; this region extends 3–4 μm from the surface when the angle of incidence is 70°–75°. Differential detection using a reference beam is used to improve upon the limited dynamic range of the 100 MHz analog-to-digital data acquisition board used to detect each probe pulse. Typically 4000 probe pulses are averaged at each delay time. The total measurement time is typically 13 s.

C. Sensitivity

The sensitivity scales with $\delta P/P$ rather than δP because the dynamic range of the photodiode is limited. Figure 5 shows calculated values of $\delta P/P$ as a function of the off-null angle. As expected, $\delta P/P$ is inversely proportional to the off-null angle. We choose the off-null angle in the experiment, typically 5°–8°, as a trade-off between sensitivity ($\delta P/P$) and signal strength (δP). At this off-null angle, off-null ellipsometry shows an order of magnitude higher sensitivity than the use of a polarizing beamsplitter.

Figure 6 shows an experimental comparison between time-resolved ellipsometry and conventional reflectivity measurements using $\hat{p}$ or $\hat{s}$ linearly polarized light. The signal oscillations caused by acoustic wave propagation decay linearly with time because the probe area defined by the overlap of the incident and outgoing probe beam decreases

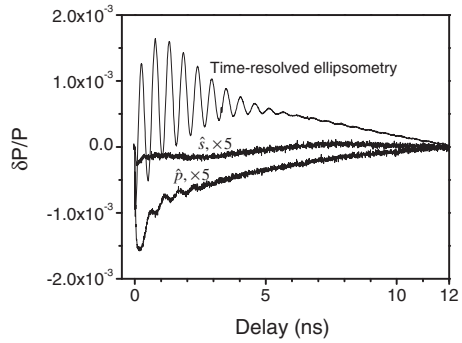

FIG. 6. The experimental quantity $\delta P/P$, at the off-null angle denoted in Fig. 5, is plotted against delay time for water. Also plotted in this panel are the pump-probe signals measured using $\hat{p}$ and $\hat{s}$ polarized light at the same angle of incidence, as would be done in a typical measurement by picosecond interferometry.

linearly with distance from the interface. Time-resolved ellipsometry provides 75 and 300 times larger signal than reflectivity using $\hat{p}$ and $\hat{s}$ linearly polarized light, respectively. Based on Eq. (1) and the model of Fig. 2, $|\delta P/P| = 1.66 \times 10^{-3}$, 1.72×10^{-5}, and 3.55×10^{-6} for time-resolved ellipsometry and reflectivity measurement using $\hat{p}$ and $\hat{s}$ linearly polarized light, respectively; the relative values of the sensitivity factors are in good agreement with experiment. The sensitivity of time-resolved ellipsometry is $\delta\Delta \approx 3 \times 10^{-7}$ deg/$\sqrt{\text{Hz}}$, which is two orders of magnitude better than a previous report of time-resolved ellipsometry using a polarizing beamsplitter and mechanical delay line.[7] This sensitivity is equivalent to a temperature excursion of ≈1 mK in a 1 nm water layer from the model calculation. (A 1 mK temperature change will causes a 10^{-7} change in density and therefore a 3×10^{-8} change in refractive index; from our model calculations, a 3×10^{-8} change in refractive index of 1 nm thick layer produces a change of phase of $\delta\Delta \approx 3 \times 10^{-7}$ from the model calculation.)

D. Transfer of heat from solid to gas

To further demonstrate this technique, we employed time-resolved ellipsometry to study a Au surface in contact with various gases at atmospheric pressure. In contrast to the situation with water, the acoustic pulse generated in the gas is mainly the result of heat transfer and associated thermal expansion of the gas. (The acoustic impedance of gas is much smaller than that of metal and most of energy in the acoustic pulse generated by the thermal expansion of Au is reflected back into the film and eventually into the substrate.) The background contribution to the signal from the Au film is readily measured in vacuum and be easily subtracted from the data, as illustrated in Fig. 7(a) for several simple gases (Ar, O_2, N_2, and He) and also a common refrigerant R134a.[23] (The molar mass of R134a is 102 g mol^{-1}.) All data in Au/gas experiments are obtained at $\theta_i = 75°$ and $\theta_p = \text{null} + 7.5°$ with 70 mW pump power, and each 5 ps time-window is averaged.

The initial drop of the signals at 0 ns$< t <$0.5 ns reveals the initial shape of the acoustic pulses generated at the solid-gas interface. The data for the refrigerant R134a show that time scale for the initial drop extends four times longer

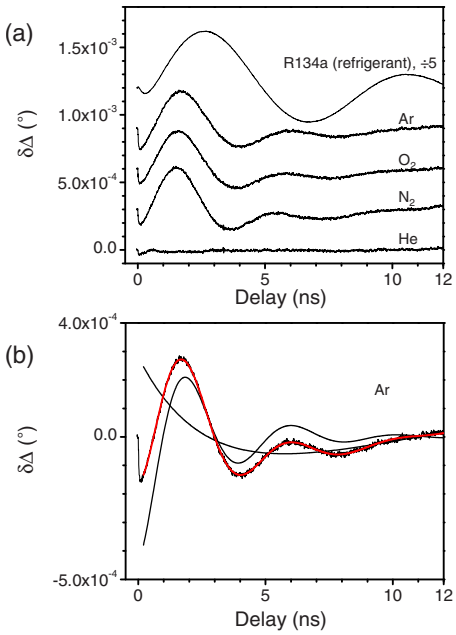

FIG. 7. (Color online) Time-resolved ellipsometry measured in various gases, both simple (Ar, O_2, N_2, and He) and complex (the refrigerant R134a), at atmospheric pressure. (a) Relative phase angle plotted against delay time in ns. Each data set is shifted vertically by 3×10^{-4} from the data for He. (b) Representative fits to the Ar data, and the contribution of each exponential and damped oscillation part are plotted.

than the other gases. This reflects the slower mean collision time between the surface and gas molecules, and the slower acoustic velocity because this refrigerant molecule is more massive than the other gas molecules. From the time scale of the initial drop and the speed of sound, the thickness of the layer related to the formation of the acoustic pulse in the gas phase is estimated to be 10 nm for He, N_2, O_2, and Ar, and 20 nm for R134a. The impulsive temperature rise of these layer is 1° for He, and 3° for N_2, O_2, and Ar, and 2° for R134a using the same model calculation as for the Au/water system. An advantage of the experiment's high time resolution is to follow the full cycles of the acoustic pulses.

We fit these and similar data sets using a combination of a damped sinusoidal oscillation and a thermal background modeled by two exponential functions, $a_1 \cos(2\pi t/a_2 + a_3) \exp(-t/a_4) + a_5(1 - \exp(-t/a_6)) \exp(-t/a_7) + a_8$, where the main parameters are the amplitude a_1 and phase of the oscillation a_3, the Brillouin frequency $1/a_2$, and the damping time a_4. The other terms in the equation involving a_5 to a_8 parameters are an empirical functional form that is intended to account for background signals from relatively slow heating and cooling of the gases. Table I shows the fitting parameters, and Fig. 7(b) shows representative fits to the Ar data. When the spatial extent of acoustic pulse is much shorter than the wavelength of light, the amplitude of the oscillation is proportional to the spatial integration of refractive index modulation inside the acoustic pulse, which is, in turn, proportional to the amount of heat transferred from solid to gas. A more meaningful number can be extracted when the amplitude a_1 is normalized by $n_{\text{gas}} - 1$; n_{gas} is the refractive index of the gas. For the data in Fig. 7(a), the normalized

TABLE I. Fitting parameters at Au/gas interfaces.

	Amplitude	Period (ps)	Phase (deg)	Damping time (ps)
O_2	4.7×10^{-4}	3980	185	2260
N_2	4.9×10^{-4}	3780	187	2270
Ar	4.5×10^{-4}	4140	185	2490
R134a	2.7×10^{-3}	7870	225	7930
He	2.7×10^{-5}	1050	142	584

amplitudes, $a_1/(n_{gas}-1)=0.9°$, 2.0°, 2.1°, 2.0°, and 2.5° for He, N_2, O_2, Ar, and R134a, respectively. These relative numbers are proportional to reports of the thermal accommodation coefficients for He, N_2, and Ar on soot surfaces, 0.13, 0.36, and 0.35, respectively (see Ref. 24).

For all rare gases at this experiment, the mean collision time τ is in the range 150 ps$<\tau<$190 ps, close to the inverse frequency of the acoustic wave.[25–27] In this regime, the dispersion and damping of an acoustic wave are a function of the rarefaction parameter, $f\tau$, where f is the frequency of acoustic wave. Dispersion is expressed by the ratio of phase velocity, $\mathrm{Re}(\Gamma)=v_0/v$, where the subscript 0 denotes the value at the low-frequency limit. Damping can be expressed as $-\mathrm{Im}(\Gamma)=\alpha\lambda_0/2\pi$, where $\alpha[=(a_4v)^{-1}]$ and $\lambda_0(=a_2v_0)$ are the absorption coefficient and acoustic wavelength, respectively.

We could not apply this analysis to the data for He because of very small signal intensity. Figure 8 shows the results of this analysis for O_2, N_2, and Ar with comparison to prior studies at 11 MHz and various pressures from 0.004 to 1 atm. The reference data from low frequency measurement reported consistent dispersion and absorption for monatomic gases such as He, Ne, Ar, Kr, and Xe, but N_2 and O_2 data reported deviations due to the additional vibration and rotation relaxation modes. In our results, all the parameters are calculated at 331 K, which is estimated to be the substrate temperature that results from steady-state heating of pump and probe laser pulses. Table II summarizes parameters of these calculations.

The difference between the low-frequency measurement of Refs. 26 and 27 and our data might reflect interface effects, or might reflect systematic errors in the fitting of the data. For the relatively weakly damped acoustic waves in R134a, the finite size of the optical beams also introduces a small systematic error by increasing the apparent damping rate.

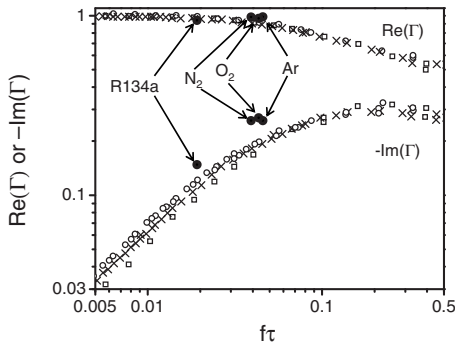

FIG. 8. Comparison to the reference values measured at 11 MHz. The absorption and dispersion of sound waves, obtained from Fig. 7 using the model described in the text, are compared to data from Refs. 26 and 27 for Ar (squares), N_2 (circles), and O_2 (crosses).

TABLE II. Parameters for the calculation of Fig. 8 at 331 K (Refs. 28 and 29).

	Speed of sound at low frequency limit (λ_0, m s^{-1})	Collision diameter (Å)	Refractive index $(n-1)$	Mean collision time (ps)
O_2	327	3.55	2.23×10^{-4}	172
N_2	350	3.70	2.47×10^{-4}	148
Ar	320	3.58	2.32×10^{-4}	189
R134a	161	5.06	1.10×10^{-3}	151
He	1290	2.15	3×10^{-5}	166

III. CONCLUSION

We have developed a time-resolved ellipsometer using an off-null detection scheme and showed that the phase of acoustic signal thermally generated by a pump optical pulse can be studied quantitatively. The sensitivity is approximately two orders of magnitude larger than obtained in reflectivity measurements. In addition to studies of heat transfer at interfaces, this technique will be useful for studying interfacial fluid and gas layers that have gradually changing physical properties near the interface.

ACKNOWLEDGMENTS

The authors thank Dr. Sung Chul Bae for many discussions and gratefully acknowledge financial support from the taxpayers of the United States through the Office of Naval Research MURI program (Grant No. N00014-07-1-0723). In addition, we thank Dr. Dong-Wook Oh and Tamlin Matthews for measurements of film thickness by RBS.

[1] Z. Ge, D. G. Cahill, and P. V. Braun, Phys. Rev. Lett. **96**, 186101 (2006).
[2] D. H. Auston and C. V. Shank, Phys. Rev. Lett. **32**, 1120 (1974).
[3] G. E. Jellison, Jr. and D. H. Lowndes, Appl. Opt. **24**, 2948 (1985).
[4] G. E. Jellison, Jr. and D. H. Lowndes, Appl. Phys. Lett. **51**, 352 (1987).
[5] H. R. Choo, X. F. Hu, M. C. Downer, and V. P. Kesan, Appl. Phys. Lett. **63**, 1507 (1993).
[6] M. Y. Frankel, Opt. Lett. **19**, 1252 (1994).
[7] D. Mounier, E. Morozov, P. Ruello, J.-M. Breteau, P. Picart, and V. Gusev, Eur. Phys. J. Spec. Top. **153**, 243 (2008).
[8] H. Yoneda, H. Morikami, K. I. Ueda, and R. M. More, Phys. Rev. Lett. **91**, 075004 (2003).
[9] V. V. Kruglyak, R. J. Hicken, M. Ali, B. J. Hickey, A. T. G. Pym, and B. K. Tanner, Phys. Rev. B **71**, 233104 (2005).
[10] R. M. Slayton and K. A. Nelson, J. Chem. Phys. **120**, 3908 (2004).
[11] D. G. Cahill, Rev. Sci. Instrum. **75**, 5119 (2004).
[12] H.-N. Lin, R. J. Stoner, H. J. Maris, and J. Tauc, J. Appl. Phys. **69**, 3816 (1991).
[13] K. E. O'Hara, X. Hu, and D. G. Cahill, J. Appl. Phys. **90**, 4852 (2001).
[14] A. R. Duggal, J. A. Rogers, and K. A. Nelson, J. Appl. Phys. **72**, 2823 (1992).
[15] C. Thomsen, H. T. Grahn, H. J. Maris, and J. Tauc, Phys. Rev. B **34**, 4129 (1986).
[16] G. Tas and H. J. Maris, Phys. Rev. B **55**, 1852 (1997).
[17] T. Pezeril, C. Klieber, S. Andrieu, and K. A. Nelson, Phys. Rev. Lett. **102**, 107402 (2009).

[18] R. M. A. Azzam and N. M. Bashara, *Ellipsometry and Polarized Light* (North-Holland, New York, 1977).
[19] H. G. Tompkins, *A User's Guide to Ellipsometry* (Academic, New York, 1993).
[20] A. Rosencwaig and A. Gersho, J. Appl. Phys. **47**, 64 (1976).
[21] N. Bilaniuk and G. S. K. Wong, J. Acoust. Soc. Am. **93**, 1609 (1993).
[22] A. Bartels, R. Cerna, C. Kistner, A. Thoma, F. Hudert, C. Janke, and T. Dekorsy, Rev. Sci. Instrum. **78**, 035107 (2007).
[23] J. Franklin, Chemosphere **27**, 1565 (1993).
[24] K. J. Daun, G. J. Smallwood, and F. Liu, ASME J. Heat Transfer **130**, 121201 (2008).
[25] J. P. M. Trusler, *Physical Acoustics and Metrology of Fluids* (Hilger, Bristol, 1991).
[26] M. Greenspan, J. Acoust. Soc. Am. **28**, 644 (1956).
[27] M. Greenspan, J. Acoust. Soc. Am. **31**, 155 (1959).
[28] *CRC Handbook of Chemistry and Physics*, 90th ed., edited by D. R. Lide (CRC, Boca Raton, 2009).
[29] B. Le Neindre and Y. Garrabos, Int. J. Thermophys. **20**, 1379 (1999).